Electrochemical and Solid-State Letters, **12** (3) B27-B30 (2009)
1099-0062/2009/12(3)/B27/4/$23.00 © The Electrochemical Society

Anion Exchange Membrane Fuel Cells: Experimental Comparison of Hydroxide and Carbonate Conductive Ions

Murat Unlu,* Junfeng Zhou, and Paul A. Kohl,z**

Chemical and Biomolecular Engineering, Georgia Institute of Technology, Atlanta, Georgia 30332-0100, USA

Anion exchange membrane fuel cells operating near room temperature using hydroxide or carbonate as the conductive ions have been demonstrated and compared. A membrane electrode assembly was fabricated using a poly(arylene ether sulfone) polymer membrane functionalized with quaternary ammonium cations. The maximum power density using hydroxide as the conductive ion was 2.1 mW/cm^2. When CO_2 was introduced to the cathode stream, the maximum power density increased to 4.1 mW/cm^2. CO_2 was shown to be materially involved in the oxygen reduction reaction at room temperature and was transported from the cathode to the anode. CO_2 was shown to be consumed at the cathode and evolved from the anode. The performance was analyzed by electrochemical impedance spectroscopy.
 [DOI: 10.1149/1.3058999]

Manuscript submitted October 31, 2008; revised manuscript received December 4, 2008. Published January 5, 2009; publisher error corrected January 15, 2009.

Proton exchange membrane fuel cells have the potential to contribute to our energy infrastructure; however, there are fundamental problems, including CO poisoning of the catalyst, expensive noble metal catalysts, perfluorinated polymer membranes, membrane and electrode degradation, excessive electro-osmotic drag of the fuel, and complex water-management issues.[1-8]

Recently, the use of anionic fuel cells based on solid polymeric anion exchange membranes (AEMs) have been demonstrated.[9-13] The use of metal-free anion exchange membranes operating at elevated pH potentially lowers or eliminates the need for platinum-based catalysts and improves the kinetics of the electrochemical reactions. However, the stability of hydrocarbon-based solid polymer anion exchange membranes is a concern at high pH due to nucleophilic attack of the fixed cation site (e.g., quaternary ammonium moieties).[14,15] To date, AEM-based fuel cells reported in the literature commonly involve hydroxide as the conducting ion; however, the involvement of carbonate ions in the fuel cell operation has been reported.[8,16] Hydroxide ions have a higher mobility than carbonate and cause fewer precipitate-related concerns; however, hydroxide is an extremely aggressive nucleophile and can degrade the anion exchange sites in the AEM. In addition, interesting observations on improvements in cell performance by soaking the membrane in carbonate solutions have been reported.[16] Previously, the viability of an AEM fuel cell using carbonate ions as the conductive ion, the carbonate cycle, was reported.[17] A carbonate cycle has several potential advantages compared to hydroxide, including operation at a lower pH (ca. 11–12) resulting in less risk of nucleophilic attack of the quaternary ammonium cations in the AEM, and potentially improved electrokinetics for the reduction of oxygen in the presence of CO_2 at the cathode.

In this work, we demonstrate and compare the performance of an AEM fuel cell based on hydroxide ions to one involving CO_2 and, presumably, carbonate ions. The membrane electrode assembly (MEA) was prepared from anion exchange polymers synthesized in this study and commercial carbon-supported Pt catalysts. The anion exchange polymers had pendant quaternary ammonium cation sites with no beta-hydrogens, thus removing the Hoffman elimination route to membrane degradation.

Experimental

The AEM used in this study was synthesized for fuel cell purposes and has been described elsewhere.[17] A brief description of the synthesis will be given here. Poly(arylene ether sulfone) was first synthesized by polycondensation reaction in DMAc/toluene cosolvent in nitrogen ambient. The polysulfone was chloromethylated by Friedel-Crafts electrophilic substitution reaction under anhydrous condition at 120°C. The chloromethyl moiety was transformed into the quaternary amino base by immersing the polymers in a solution consisting of 45% trimethylamine solution at room temperature for two days. The final polymer was cast from DMF solvent on Teflon plates to form a flexible AEM. The membranes were 100 to 200 μm thick. For ex situ measurements, the mobile chloride in the synthesized AEMs was replaced by hydroxide or carbonate by immersing the membranes in aqueous potassium hydroxide (1 M) or sodium carbonate (1 M) solutions for one day. The physical properties of these AEMs are summarized in Table I.

Electrodes were fabricated using commercial carbon-supported platinum (Pt/C) catalysts, which were 20% platinum by mass (E-TEK). The catalyst ink was prepared by sonicating a mixture of Pt/C catalyst powder and poly(arylene ether sulfone) ionomer in a DMF and water cosolvent. The catalyst slurry was painted on hydrophobic Toray carbon paper (TGPH-090) and dried at room temperature. The catalyst and ionomer loadings were 1 and 0.8 mg/cm^2, respectively. The electrodes were pressed onto the AEMs with 5 kg/cm^2 pressure at room temperature and held for 5 min. The dry thickness of AEM was 140 μm. Once the MEAs were assembled, they were soaked in 0.5 M Na_2CO_3 solution for 5 h to exchange Cl^- ions in the electrode ionomers with CO_3^{2-}. For the hydroxide cycle tests, the MEAs were run in fuel cell mode with humidified H_2/O_2 feeds (100% relative humidity). The fuel cell was operated at constant potential, 600 mV, for 24 h in order to convert the conductive ions from CO_3^{2-} to OH^- ions. The average current during this 24 h period was 1.9 mA/cm^2. The total charge passed during this 24 h period corresponds to replacing the total ionic content of the membrane 24 times over. During the transient period, the humidity and ion content were changed, which generally led to a higher current for a short time. These non-steady-state effects were not investigated at this point.

Table I. Physical properties of the membranes used in this study.

	Ionic functional group	Conductivity (mS/cm)	Water-uptake (%)
AEM-1	$-N^+(CH_3)_3OH^-$	21.21	63.86
AEM-2	$[-N^+(CH_3)_3]_2CO_32^-$	9.91	46.06

Water uptake = 100% × $(W_{hyd} - W_{dry})/W_{dry}$, where W_{hyd} is the mass of the fully hydrated membrane and W_{dry} is the mass of the fully dehydrated membrane. Ionic conductivity was measured in 1 M NaOH or Na_2CO_3 solution at 25°C.

* Electrochemical Society Student Member.
** Electrochemical Society Fellow.
z E-mail: kohl@gatech.edu

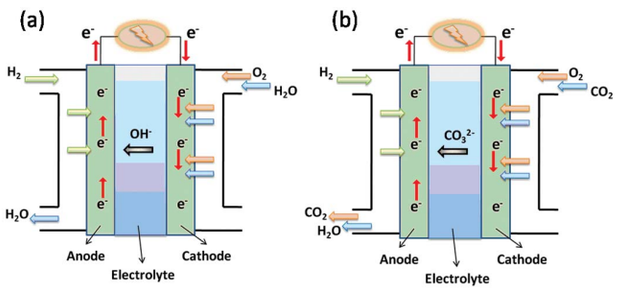

Figure 1. (Color online) Diagram of fuel cells operating on (a) the hydroxide cycle and (b) the carbonate cycle.

Electrochemical measurements were performed using a PAR 2273 potentiostat/galvanostat. Fuel cell tests were conducted at 25°C at ambient pressures. The anode and cathode feed streams were saturated with moisture (100% humidified). All gases were high purity industrial grade obtained from Airgas. Electrochemical impedance spectra were measured after recording the polarization curves, in the constant voltage mode by sweeping frequency from 10 mHz to 10 kHz. The amplitude of the alternating voltage for the impedance spectra was 10 mV.

Results and Discussion

Charge transport in an AEM fuel cell is provided by negative ions migrating from the cathode to the anode through the AEM, as depicted in Fig. 1. In order to compare the carbonate and hydroxide systems, a single MEA was fabricated and tested under different cathode gas flow conditions. Table II shows the test conditions for three experiments. In each test, the anode stream was the same: 100% humidified hydrogen.

In test 1, the fuel cell performance was evaluated using only hydroxide ions as the conductive species by virtue of the oxygen/water feed at the cathode (the hydroxide cycle). The gas flow rate of the humidified oxygen was 3 sccm. All gas lines were well purged of impurities before operation. The cells were run for many hours to ensure steady-state conditions. The open-circuit voltage (OCV) at steady state was 970 mV, and the maximum power density obtained was 2.4 mW/cm^2, as shown in Fig. 2. Oxygen reduction at the cathode takes place in the presence of water resulting in the production of hydroxide ions (Eq. 1). The hydroxide ions migrate through the AEM and combine with protons produced through the oxidation of hydrogen at the anode producing water, as shown in Eq. 2

$$\tfrac{1}{2}O_2 + \tfrac{1}{2}H_2O + 2e^- \rightarrow 2OH^- \quad E_0 = 0.40\ \text{V[standard hydrogen electrode (SHE)]} \qquad [1]$$

$$H_2 + 2OH^- \rightarrow 2H_2O + 2e^- \quad E_0 = 0.83\ \text{V(SHE)} \qquad [2]$$

At low cell voltages (e.g., <500 mV), the cell resistance is smaller than at high voltages, as shown by the two linear regions in the *I-V* curve in Fig. 2. One possible reason may be the back-diffusion of water from the anode to the cathode at higher currents. Although the cathode stream was humidified, the cathode had a hydrophobic character due to the Toray paper. The water produced at the anode may also improve the conductivity of the AEM by increasing its water content. Water analysis will be the subject of future detailed reports with these membranes. The decrease in resistance at higher current was confirmed by impedance spectroscopy, as discussed later in this section. Also, the mass transport limitation of water and improved performance at high current density are consistent with other hydroxide-conducting AEM fuel cell reports.[12]

Table II. Gas compositions and corresponding conducting ions.

Test	Conducting ion	Anode	Cathode
1	OH^-	H_2 (humidified)	O_2 (humidified)
2	CO_3^{2-} and OH^-	H_2 (humidified)	$O_2 + CO_2$ (humidified)
3	CO_3^{2-}	H_2 (humidified)	CO_2 (dry)

Flow rates are 6, 3, and 6 mL/min for hydrogen, oxygen, and carbon dioxide, respectively.

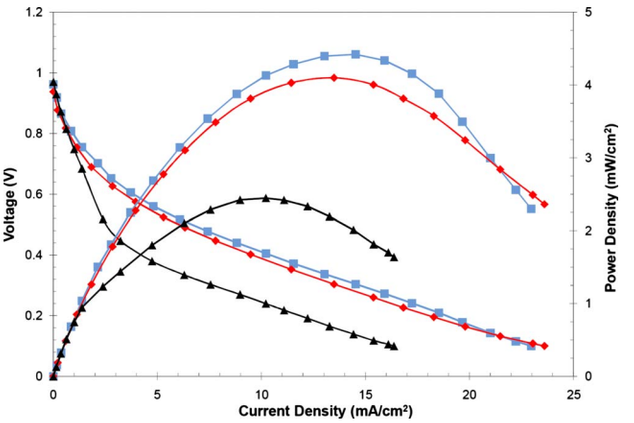

Figure 2. (Color online) Polarization curves of the same MEA for the cathode stream with (▲) humidified O_2 (test 1), (●) humidified $O_2 + CO_2$ (test 2), and (■) dry $O_2 + CO_2$ (test 3). The anode feed is humidified H_2 in all conditions.

The same MEA was studied using carbon dioxide in the cathode stream, as described by test 2 in Table II. The MEA was preloaded with carbonate ions by soaking in Na_2CO_3 solution. The flow rate of CO_2 was 6 sccm, and the oxygen flow rate remained at 3 sccm. The OCV was 938 mV. The maximum power density obtained increased to 4 mW/cm^2, about twice the power density compared to the oxygen only cathode feed in test 1. It is important to note that the addition of CO_2 to the cathode stream lowers the partial pressure of oxygen at the cathode. The humidification in the cathode stream was unchanged. Thus, the CO_2 in the cathode feed is responsible for an increase in the current.

Several experiments were performed to further test the participation of CO_2 in the cycle. The cell response to a step change in the CO_2 content in the cathode stream is shown in Fig. 3. The cell was operated at constant potential (600 mV) and 6 sccm of CO_2 was

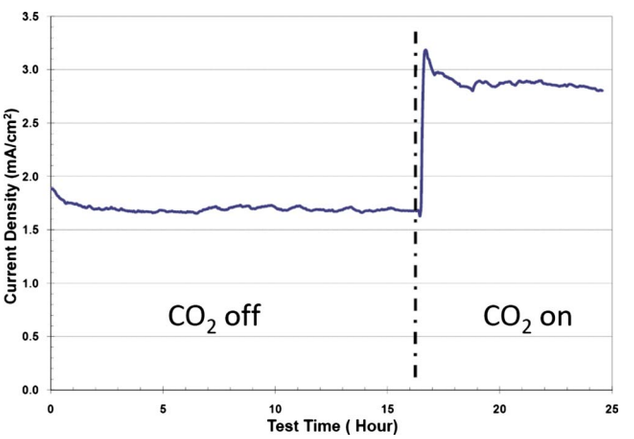

Figure 3. (Color online) Current density of fuel cell operating at 600 mV and 25°C with and without CO_2 in the cathode stream. The anode feed is humidified H_2.

added to the 3 sccm humidified oxygen flow in the cathode feed. The current quickly increased when the oxygen feed was diluted with CO_2. When the CO_2 flow was terminated, the current returned to a lower value.

The effect of oxygen crossover from the cathode to the anode by diffusion was considered. If oxygen crossover to the anode limited the current, then a reduction in the partial pressure of oxygen at the cathode could cause an increase in performance due to less crossover. In a separate experiment, a humidified oxygen feed was used at the cathode and the cell was operated at steady state. The current at 600 mV was 3.3 mA. The oxygen stream (3 sccm) was diluted with nitrogen with a flow rate of 6 sccm. The current quickly dropped by 40% to 2.1 mA (600 mV constant cell potential). The humidified oxygen stream was then diluted with CO_2 at the same flow rate as with nitrogen, 6 sccm. The current at 600 mV increased to 5.8 mA. If the effect of the diluting gas were simply to lower the partial pressure of oxygen and reduce crossover, then both nitrogen and carbon dioxide would have the same effect.

According to a previously proposed carbonate cycle (Fig. 1b), CO_2 reacts with O_2 forming carbonate ions that migrate from the cathode to the anode through the AEM.[13] CO_3^{2-} then reacts with hydrogen ions at the anode to form CO_2

$$2CO_2 + O_2 + 4e^- \rightarrow 2CO_3^{2-} \quad [3]$$

$$H_2 + CO_3^{2-} \rightarrow H_2O + CO_2 + 2e^- \quad [4]$$

It is important to note in test 2 that there is H_2O present in the O_2 and CO_2 cathode stream. Thus, it is also possible for oxygen to be reduced with H_2O to hydroxide ions. Indeed, the hydroxide and carbon dioxide will be acid-base equilibrium in all cases. The consumption rate of water and carbon dioxide at the cathode was not measured in these experiments, and a detailed mass balance is in progress.

The importance of water in the cathode feed was investigated in test 3 (Table II and Fig. 2). In test 3, the cathode feed was changed from humidified oxygen and carbon dioxide to dry oxygen (3 sccm) and carbon dioxide (6 sccm). The anode feed remained humidified hydrogen. The anode humidification was necessary in order to maintain adequate ionic conductivity in the MEA. The cell polarization curve was collected after 1 h operation at 600 mV, and is shown in Fig. 2. The OCV was 962 mV. The maximum power density increased to 4.4 mW/cm^2. This experiment confirms that carbon dioxide is involved in the cathodic reaction because there is no water intentionally added to the cathode feed. Although it is possible for water to diffuse through the AEM, one would not expect the current to increase by eliminating most of the water from the cathode feed, if water were the dominant species involved in oxygen reduction.

The results presented in Fig. 2 and 3 show an enhancement in the fuel cell performance with CO_2 in the cathode feed. If CO_2 were consumed with oxygen at the cathode producing carbonate ions, which migrate to the anode, then CO_2 would be produced at the anode. If CO_2 were not involved in cathode reaction or carbonate were not a component of the ionic transport, then no CO_2 should be formed at the anode, except for diffusional crossover. If hydroxide was the only conductive ion, then water would be the only product at the anode.

The production of CO_2 in the anode compartment was demonstrated by flowing the anode product stream through a calcium hydroxide solution. If CO_2 was present in the anode gas stream, then a $CaCO_3$ precipitate would be observed. The cell was operated at 4 mA/cm^2 with a 3 sccm hydrogen flow rate at the anode and a cathode flow consisting of 3 sccm O_2 and 6 sccm CO_2. The cell was flushed and operated long enough to ensure the anode compartment was completely free of ambient CO_2 gas at start-up. The anode exhaust gas was bubbled through a 0.01 M $Ca(OH)_2$ solution. Within seconds, a milky precipitate ($CaCO_3$) was observed in the $Ca(OH)_2$ solution. The amount of precipitate increased with time as the cell operated. This test clearly shows the presence of CO_2 in the anode exhaust.

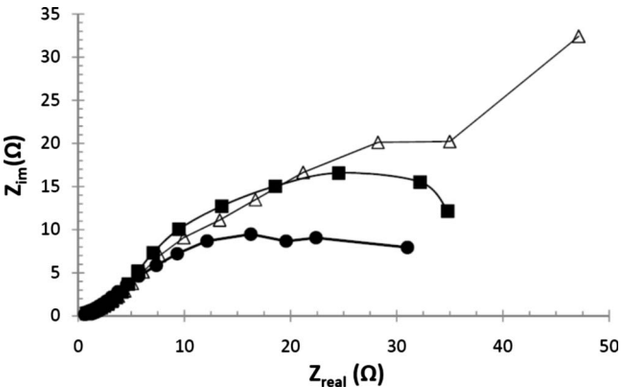

Figure 4. EIS spectra at (■) 800, (△) 700, and (●) 300 mV for test 1 conditions.

The possible diffusion of CO_2 through the membrane from the cathode stream to the anode stream was also considered. Control experiments were performed to verify that the CO_2 observed in the anode stream was indeed due to the electrochemical oxidation of hydrogen in the presence of carbonate and the CO_2 crossover was insignificant. The same cell and membrane were configured with identical gas flow conditions to the one described above except the cell current was held at zero. The anode gas was first purged of any residual gases by using the same gas flow rate (3 sccm hydrogen). The cathode gas mixture was again 3 sccm oxygen and 6 sccm carbon dioxide. The anode exhaust was bubbled through the $Ca(OH)_2$ test solution, and no precipitate was observed in the $Ca(OH)_2$ solution. This shows that the appearance of CO_2 in the anode compartment is electrochemically generated and not due to diffusion.

The overall performance of these cells is modest compared to comparable AEM cells. However, the performance is higher than previous attempts at room-temperature carbonate cells.[13] Clearly these MEAs have not been optimized and work is underway to fabricate better electrodes using the ionomers synthesized here. As a start to an understanding of the origin of the power losses in these cells, electrochemical impedance spectroscopy (EIS) was used. It has been generally shown that the cell impedance is determined by the cathode.[18,19] Figures 4 and 5 show EIS spectra at various voltages for a cell run under tests 1 and 2 conditions, respectively. For the hydroxide cycle in test 1 at 800 mV, the spectrum is a generic semicircle loop. Typically, the difference between the *x*-intercept

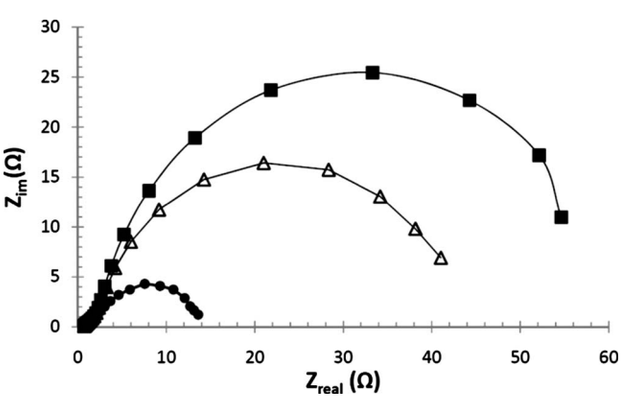

Figure 5. EIS spectra at (■) 800, (△) 700, and (●) 300 mV for test 2 conditions.

values of the two ends of the semicircle is the charge transfer resistance and the high-frequency *x*-intercept corresponds to the MEA resistance.[20,21] This spectrum shows that the losses due to charge-transfer resistance are more prominent than the MEA resistance. At 700 mV, the spectrum is significantly different from the one at 800 mV. At high frequencies, the imaginary resistance is lower at 700 mV than at 800 mV. At low frequencies, the imaginary and corresponding real resistances increase when the voltage decreases from 800 to 700 mV. At 300 mV, both high- and low-frequency regions possess lower imaginary and real resistance components than at 700 mV. The appearance of higher resistance at low frequency is generally attributed to complications due to mass transfer effects.[22] The details of these mass transfer effects will be reported in further investigations.

The identical EIS spectra were collected for test 2 conditions in which CO_2 (6 sccm) was introduced to the cathode stream. EIS spectra exhibited a typical semicircle loop at all voltages. The size of the semicircle pattern is substantially smaller at lower voltages (shown in Fig. 5). This behavior is attributed to charge-transfer resistance, which is mainly determined by interfacial charge-transfer kinetics, ionic conductivity, and diffusion limitations in the catalyst layer.[21] This charge-transfer resistance is quite high likely due to the nonoptimized electrode construction.

The ex situ electrode conductivity was larger when the membrane was soaked in hydroxide than when soaked in carbonate solution. This was expected due to the higher conductivity of hydroxide than carbonate. However, the higher hydroxide conductivity did not translate into higher fuel cell performance because the electrode and mass transfer limitations dominated, as seen in the EIS results above. The ionic resistance of carbonate and hydroxide in the MEA were compared by in situ EIS measurements. On the basis of the results presented above, the fuel cell at test 2 conditions was assumed to function mostly with carbonate ions while hydroxide was the only conducting ion in test 1. The contribution of the MEA resistance was determined from the high-frequency *x*-intercepts in the EIS spectra for tests 1 and 2 conditions. For the hydroxide cycle in test 1, the resistance gradually decreases from 0.75 to 0.55 Ω as the operating voltage decreases from 900 to 300 mV. This change in the resistance could be attributed to hydration of the MEA at high-current. The resistance at high frequency intercept is almost constant (0.75 Ω) at various operating voltage in test 2. One likely source of the resistance differences is the different hydration degrees in two test conditions due to different water stoichiometries of hydroxide and carbonate cycles (as seen in Eq. 1-4).

Conclusion

AEM fuel cells were demonstrated using hydroxide or carbonate as the conductive ions. Direct comparison between the fuel cell operating with hydroxide and carbonate ions reveals that carbonate cycle is superior with the power density of 4.1 mW/cm^2 to ones using hydroxide with 2.4 mW/cm^2 in given operating conditions. The product evaluation confirms CO_2 consumption in the cathode and generation in the anode. It is shown that CO_2 improves the cell performance by reacting with O_2. Steady-state polarization curves and EIS characterization provide consistent and supporting evidences for the viability of the carbonate cycle.

Georgia Institute of Technology assisted in meeting the publication costs of this article.

References

1. J. Larminie and A. Dicks, *Fuel Cell Systems Explained*, Wiley, Chichester (2003).
2. K. Yasuda, A. Taniguchi, T. Akita, T. Ioroi, and Z. Siroma, *Phys. Chem. Chem. Phys.*, **8**, 746 (2006).
3. T. V. Nguyen and R. E. White, *J. Electrochem. Soc.*, **140**, 2178 (1993).
4. H. Meng, M. Wu, X. X. Xu, M. Nei, Z. D. Wei, and P. K. Shen, *Fuel Cells*, **6**, 447 (2006).
5. E. H. Yu and K. Scott, *J. Power Sources*, **137**, 248 (2004).
6. P. Zegers, *J. Power Sources*, **154**, 497 (2006).
7. V. Rao, Hariyanto, C. Cremers, and U. Stimming, *Fuel Cells*, **7**, 417 (2007).
8. J. H. Wee and K. Y. Lee, *J. Power Sources*, **157**, 128 (2006).
9. T. N. Danks, R. C. T. Slade, and J. R. Varcoe, *J. Mater. Chem.*, **13**, 712 (2003).
10. J. R. Varcoe and R. C. T. Slade, *Fuel Cells*, **5**, 187 (2005).
11. J. R. Varcoe, R. C. T. Slade, E. Lam HowYee, S. D. Poynton, D. J. Driscoll, and D. C. Apperley, *Chem. Mater.*, **19**, 2686 (2007).
12. J. R. Varcoe, R. C. T. Slade, G. L. Wright, and Y. Chen, *J. Phys. Chem. B*, **110**, 21041 (2006).
13. C. M. Lang, K. Kim, and P. A. Kohl, *Electrochem. Solid-State Lett.*, **9**, A545 (2006).
14. V. Neagu, I. Bunia, and I. Plesca, *Polym. Degrad. Stab.*, **70**, 463 (2000).
15. A. A. Zagorodni, D. L. Kotova, and V. F. Selenemev, *React. Funct. Polym.*, **53**, 157 (2002).
16. L. A. Adams, S. D. Poynton, C. Tamain, R. C. Slade, and J. R. Varcoe, *ChemSusChem*, **1**, 79 (2008).
17. J. Zhou, M. Unlu, and P. A. Kohl, *J. Power Sources*, Submitted.
18. M. Ciureanu and H. Wang, *J. Electrochem. Soc.*, **146**, 4031 (1999).
19. B. Andreaus, A. J. McEvoy, and G. G. Scherer, *Electrochim. Acta*, **47**, 2223 (2002).
20. I. D. Raistrick, *Electrochim. Acta*, **35**, 1579 (1990).
21. T. E. Springer, T. A. Zawodzinski, M. S. Wilson, and S. Gottesfeld, *J. Electrochem. Soc.*, **143**, 587 (1996).
22. V. A. Paganin, C. L. F. Oliveira, E. A. Ticianelli, T. E. Springer, and E. R. Gonzalez, *Electrochim. Acta*, **43**, 3761 (1998).